ACS APPLIED MATERIALS & INTERFACES

Research Article

www.acsami.org

Impact of the Cation Composition on the Electrical Performance of Solution-Processed Zinc Tin Oxide Thin-Film Transistors

Yoon Jang Kim,[†] Seungha Oh,[†] Bong Seob Yang,[†] Sang Jin Han,[†] Hong Woo Lee,[†] Hyuk Jin Kim,[†] Jae Kyeong Jeong,*[,‡] Cheol Seong Hwang,*[,†] and Hyeong Joon Kim*[,†]

[†]Department of Materials Science and Engineering, and Inter-university Semiconductor Research Center, Seoul National University, Seoul 151-742, Republic of Korea

[‡]Department of Materials Science and Engineering, Inha University, Incheon 402-751, Republic of Korea

Supporting Information

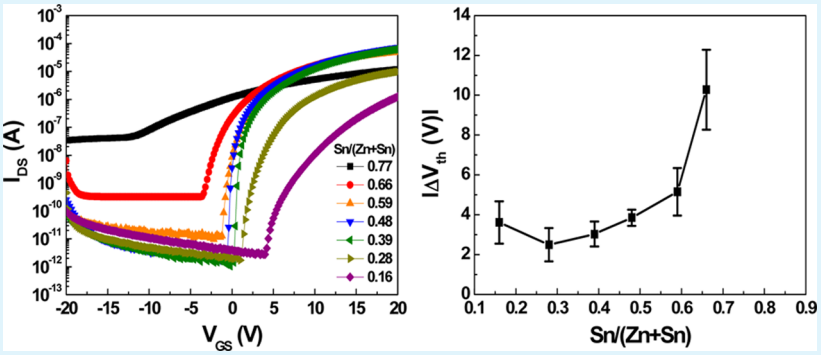

ABSTRACT: This study examined the structural, chemical, and electrical properties of solution-processed $(Zn,Sn)O_3$ (ZTO) films with various Sn/[Zn+Sn] ratios for potential applications to large-area flat panel displays. ZTO films with a Zn-rich composition had a polycrystalline wurtzite structure. On the other hand, the Sn-rich ZTO films exhibited a rutile structure, where the Zn atom was speculated to replace the Sn site, thereby acting as an acceptor. In the intermediate composition regions (Sn/[Zn+Sn] ratio from 0.28 to 0.48), the ZTO films had an amorphous structure, even after annealing at 450 °C. The electrical transport properties and photobias stability of ZTO thin film transistors (TFTs) were also examined according to the Sn/[Zn+Sn] ratio. The optimal transport property of ZTO TFT was observed for the device with an amorphous structure at a Sn/[Zn+Sn] ratio of 0.48. The mobility, threshold voltage, subthreshold swing, and on/off current ratio were 4.3 $cm^2/(V\,s)$, 0 V, 0.4 V/decade, and 4.1×10^7, respectively. In contrast, the device performance for the ZTO TFTs with either a higher or lower Sn concentration suffered from low mobility and a high off-state current, respectively. The photoelectrical stress measurements showed that the photobias stability of the ZTO TFTs was improved substantially when the ZTO semiconducting films had a lower oxygen vacancy concentration and an amorphous structure. The relevant rationale is discussed based on the phototransition and subsequent migration mechanism from neutral to positively charged oxygen vacancies.

KEYWORDS: *zinc tin oxide, thin film transistor, solution process, mobility, stability*

1. INTRODUCTION

Metal-oxide (MO) thin-film transistors (TFTs) have attracted considerable interest as a strong candidate for realizing flexible, transparent, large-area, low-cost electronic devices, including active-matrix liquid crystal displays (LCDs), organic-light emitting diodes (OLEDs), electronic paper, and smart identification cards. These emerging applications are enabled by the promising properties of oxide-based TFTs, including high mobility, good transparency, low processing temperature, and reasonable stability compared to amorphous silicon TFTs.[1] MO TFTs are fabricated mainly using vacuum-based deposition processes, such as magnetron sputtering,[2] pulsed laser deposition (PLD),[3] and atomic layer deposition (ALD).[4] However, most vacuum-based processes are expected to have some problems in obtaining the compatibility with very large flat panel displays, because of the very high cost of fabrication. Solution-based processes have become a viable alternative to vacuum-based processes, because they offer process simplicity, low manufacturing cost, and potentially high throughput.[5,6]

The most researched thin-film material for TFT applications is $InGaZnO_4$ (IGZO), which has a high carrier (electron) mobility (μ_e) (>10 $cm^2V^{-1}s^{-1}$, for 50 nm thick film), even in an amorphous material, which is generally not the case for other materials, such as amorphous Si (μ_e < 1 $cm^2V^{-1}s^{-1}$, for a film ~150 nm thick). According to these primary merits of IGZO, ultrahigh-resolution LCDs and large-area OLED products

Received: May 29, 2014
Accepted: August 4, 2014
Published: August 4, 2014

adopting IGZO-TFTs are commercially available.[7] The high overlap of In 5s orbitals, which mainly constitute the conduction band of the amorphous IGZO network, and their nondirectionality are responsible for the high μ_e in this material.[1,8] The In atom plays the role as a carrier concentration and mobility enhancer, whereas Ga generally plays the opposite role. This can be attributed to the weak and strong binding of In−O bonds and Ga−O bonds, respectively. Therefore, appropriate control of the In/Ga ratio is the most critical parameter for achieving the desired properties from the IGZO-TFTs.[9,10] Nevertheless, the complicated composition of IGZO makes precise control of the composition and oxygen stoichiometry over a very large area difficult. In addition, the rarity of In and Ga has revitalized the exploration of zinc tin oxide (ZTO) for use in the channel layer of TMO TFTs. The Sn 5s orbital in ZTO plays a role similar to that of the In 5s orbital in IGZO.[11] Therefore, many studies have reported the effects of the chemical precursor, composition, and annealing temperature of ZTO-based films. The transport properties of the resulting ZTO-based TFT devices have also been reported.[12−20] The earlier compositional effect was studied for the sputtered ZTO TFTs by Hoffman and co-workers.[12] High field-effect mobility (~30 $cm^2/(V\ s)$) and a reasonable on/off (I_{on}/I_{off}) ratio (~10^6) were achieved for the TFTs with the channel composition of Zn:Sn = 50:50 at annealing temperatures ranging from 400 °C to 600 °C. The in-depth combinatorial study of ZTO TFTs was reported by McDowell et al. They fabricated the ZTO TFTs with various Zn:Sn ratio by cosputtering the ZnO and SnO_2 target.[13] Two maximum mobilities of 10−12 $cm^2/(V\ s)$ and 8−11 $cm^2/(V\ s)$ were obtained for TFTs with the cation composition of Zn:Sn = 25:75 and 80:20, respectively, which contradicted the earlier result reported by Hoffman et al. The solution-based process is desirable for the low-cost and mass production of large-area devices, as previously mentioned. In this regard, Jeong et al. reported the effects of the incorporated Sn concentration on the transfer characteristics of solution-processed ZTO TFTs with a channel layer ~35 nm thick.[17] The μ_e and off-state current of the ZTO TFTs increased with increasing Sn concentration, which was attributed to the donor-like behavior of Sn atoms in a semiconducting ZTO film. Kim et al. examined the effects of the Sn concentration on the drain current−gate voltage (I_{DS}−V_{GS}) performance and electrical stability of solution-processed ZTO TFTs with channel layers 30−40 nm thick under dark conditions.[18] They reported that the dark condition stability of the TFTs degraded with decreasing Sn concentration. This instability was attributed to the electric-field induced oxygen adsorption from the air ambient to the back surface of the ZTO film, which modifies the carrier concentration in the channel layer. Such oxygen adsorption was believed to be enhanced when the zinc concentration was high (Sn concentration was low), because of the higher oxidation potential of Zn than Sn. On the other hand, these studies did not provide any direct information on the donor-like behavior of Sn in the ZTO material. In addition, very little is known regarding the influence of the Sn concentration on the photobias instability of solution-processed ZTO TFTs,[14−20] even though the light-induced instability of MO TFTs is a technically important issue.[7]

This study examined the effects of the Sn concentration on the various physical properties of the ZTO films, as well as the accompanying transport properties and photobias instability of solution-processed ZTO TFTs. The structural and chemical properties of ZTO films were strongly dependent on the Sn concentration. The ZTO films with Zn-rich and Sn-rich compositions crystallized with the wurtzite and rutile structures, respectively, after annealing at 450 °C for 1 h in air, whereas the ZTO films with a Sn/Zn ratio ~1 maintained the amorphous structure. The Sn in a ZTO film with a Zn-rich composition was identified as a carrier generator (donor center). In contrast, the Zn atoms in the rutile-structured ZTO films with a Sn-rich composition work as an acceptor center. The optimal photobias stability of the ZTO TFTs was determined from the microstructure of the ZTO film rather than from the chemical defects of ZTO films.

2. EXPERIMENTAL PROCEDURE

The precursor solution was prepared by dissolving zinc acetate [$Zn(CH_3COO)_2$, Aldrich] and tin(II) chloride dihydrate [$SnCl_2{\cdot}2H_2O$, Aldrich], respectively, in 2-methoxy ethanol solvent. The total concentration of the metal precursor in the solution was fixed to 0.3 M, and the molar ratio of Sn/[Zn+Sn] was varied from 0.2 to 0.9. The precursor solution was stirred for 1 h at 60 °C and filtered through a 0.22 μm syringe filter before spin coating. Heavily doped *p*-type Si and a 100-nm-thick thermally grown SiO_2 layer were used as a substrate and a gate oxide in the ZTO TFTs, respectively. The substrate was cleaned sequentially with acetone, isopropanol, and deionized water for 10 min, followed by exposure to ultraviolet light and ozone for 20 min to produce a hydrophilic surface. The ZTO solutions were spin-coated at 500 rpm for 5 s and then at 2000 rpm for 30 s. The resulting ZTO precursor film was dried at 150 °C for 10 min to evaporate the solvent and then annealed at temperatures at 450 °C for 1 h in air. The thickness of the ZTO film after the thermal annealing was 22−29 nm. Tin-doped indium oxide (ITO), as the source and drain electrodes (S/D), was deposited by dc magnetron sputtering and patterned through a metal shadow mask. The width (W) and length (L) of the fabricated device was 1000 and 300 μm, respectively. Finally, the fabricated device was encapsulated with poly(methyl methacrylate) (PMMA, MicroChem A4) to prevent dynamic interactions between the channel layer and ambient oxygen/moisture.

The chemical compositions of the ZTO films were examined by X-ray fluorescence (XRF, Thermo Scientific) spectroscopy, for which the atomic concentrations were calibrated by proton-induced X-ray emission. The structural properties of the ZTO films were evaluated by grazing incidence X-ray diffraction (GIXRD, X'Pert PRO, PANalytical) using Cu Kα radiation and high-resolution transmission electron microscopy (HRTEM, FEI, Tecnai F20). The chemical state of the ZTO films was examined by X-ray photoelectron spectroscopy (XPS, SIGMA PROBE, ThermoVG). For XPS analysis, the ZTO films were inserted in the XPS chamber within 30 min after the post-annealing process at 450 °C. The back surface region (~5 nm) of ZTO films was etched by the plasma in situ etching in XPS chamber to remove the surface contamination. The Sn/[Zn +Sn] ratios of the surface layer of ZTO films were identical within the error range of XPS measurement to those of the bulk ZTO films. In this study, the O 1s XP spectra were deconvoluted into three asymmetric Lorenzian−Gaussian peaks with Shirley background. The curve-fitting were performed for all spectra with the full width at half-maximum (fhwm) and the ratio of Gaussian to Lorentzian parameters fixed as constant, while allowing the peak binding energies and areas to vary. The carrier density of the ZTO film was evaluated

from Hall effect measurements using the van der Pauw configuration. The electrical characteristics were measured using a Model HP 4155A (Agilent) semiconductor parameter analyzer at room temperature in air.

3. RESULTS AND DISCUSSION

Figure 1 shows the GIXRD patterns of the ZTO films with various Sn concentrations. The ZnO and SnO_2 phases were

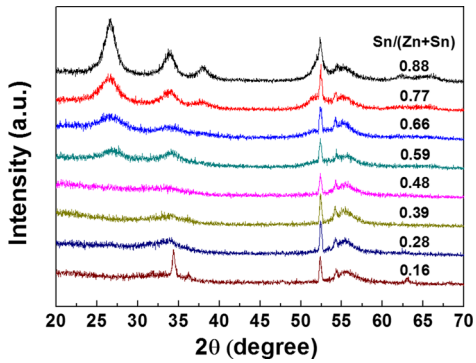

Figure 1. XRD patterns of the ZTO thin films as a function of the incorporated Sn concentration.

clearly seen at the low and high Sn contents, respectively. First, the ZTO film with an Sn/[Zn+Sn] ratio of 0.16 has a sharp peak at 2θ = 34.35°, except for the (311) plane at 54.5° from the Si substrate, indicating that it has a polycrystalline structure with a preferential orientation. Crystalline ZnO has a wurtzite structure, which belongs to the hexagonal system ($P6_3mc$, No. 186).[21] In the case of pure ZnO, the (002) peak was expected to appear at $2\theta \approx 34.44°$. Therefore, the peak of the ZTO film at an Sn/[Zn+Sn] ratio of 0.16 was assigned to the (002) reflection of wurtzite ZnO. The ~0.09° smaller 2θ angle of the (002) reflection for this ZTO film can be explained by the substitutional doping of Sn atoms in ZnO. Sn^{4+} has a larger ionic radius (69 pm for a coordination number of 6) than Zn^{2+} (60 pm for a coordination number of 4). The increasing Sn concentration in the range of the Sn/[Zn+Sn] ratio from 0.28 to 0.48 resulted in amorphous film. The diffuse scattering peak attributed to the amorphous phase near ~33° shifted toward lower 2θ angles, suggesting an expansion in the average cation-oxygen distance. This can be understood from the higher doping concentration of Sn^{4+} with a larger ionic radius. In contrast, the Sn-rich ZTO films (Sn/[Zn+Sn] ≥ 0.59) showed the typical diffraction patterns from polycrystalline materials with no preferred growth direction. For example, the ZTO film with a Sn/[Zn+Sn] ratio of 0.88 had three diffraction peaks, corresponding to the (110), (101), and (200) reflections of rutile SnO_2. In the Sn-rich region, the intensities of these diffraction peaks increased gradually and the fwhm decreased with increasing Sn concentration in the ZTO films. This suggests that the effective grain size of the ZTO film increases with increasing Sn concentration. The mean crystallite size (d) of these samples can be estimated using the fwhm of the (002) peak of wurtzite ZnO and the (110) peak based on Scherrer's formula:[22]

$$d = \frac{0.9\lambda}{B \cos \theta_B} \quad (1)$$

where λ is the X-ray wavelength (1.541 Å, Cu Kα radiation), θ_B is the Bragg diffraction angle, and B is the fwhm of the (002) and (110) peaks. The mean crystallite size of the ZTO film increased from 1.64 nm to 4.59 nm with increasing Sn concentration from 0.59 to 0.88, whereas the average grain size of the Sn-deficient ZTO film at the Sn/[Zn+Sn] ratio of 0.16 was estimated to be larger (~9.8 nm). The tendency of amorphous film formation in the intermediate compositions of the Sn/[Zn+Sn] ratio from 0.28 to 0.48 would be attributed to the larger nucleation and diffusion energy barriers due to the different crystallographic arrangement between wurzite and rutile crystal structure. The wurzite ZnO structure is based on the corner sharing of tetrahedral ZnO_4, while the rutile SnO_2 consists of the edge-sharing SnO_6 octahedra. Thus, the formation of intermixed ilmenite $ZnSnO_3$ between two different crystal structures was reported to require the high annealing temperature (~650 °C).[15]

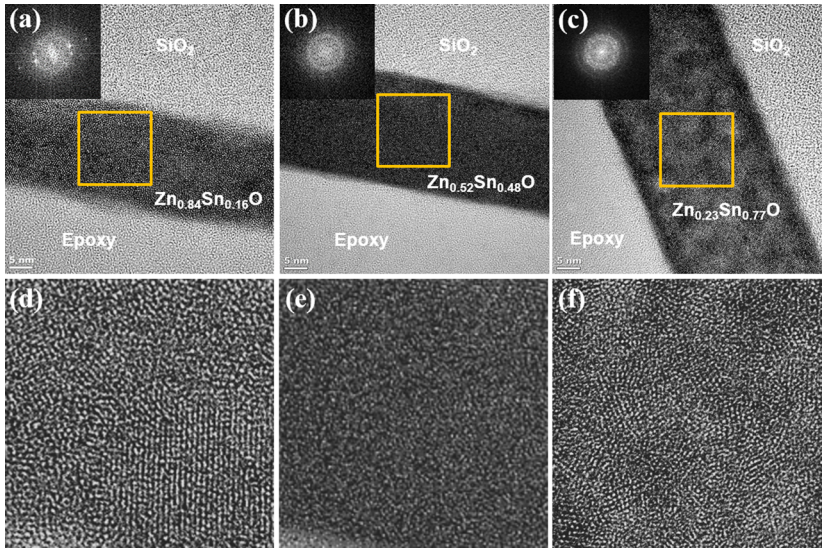

Figure 2. (Upper panels) Cross-section TEM images of ZTO thin films with a Sn/[Zn+Sn] ratio of (a) 0.16, (b) 0.48, and (c) 0.77 (the selected area diffraction pattern of each film is shown as an inset in each panel). (Lower panels) High-resolution image of ZTO films with a Sn/[Zn+Sn] of (d) 0.16, (e) 0.48, and (f) 0.77.

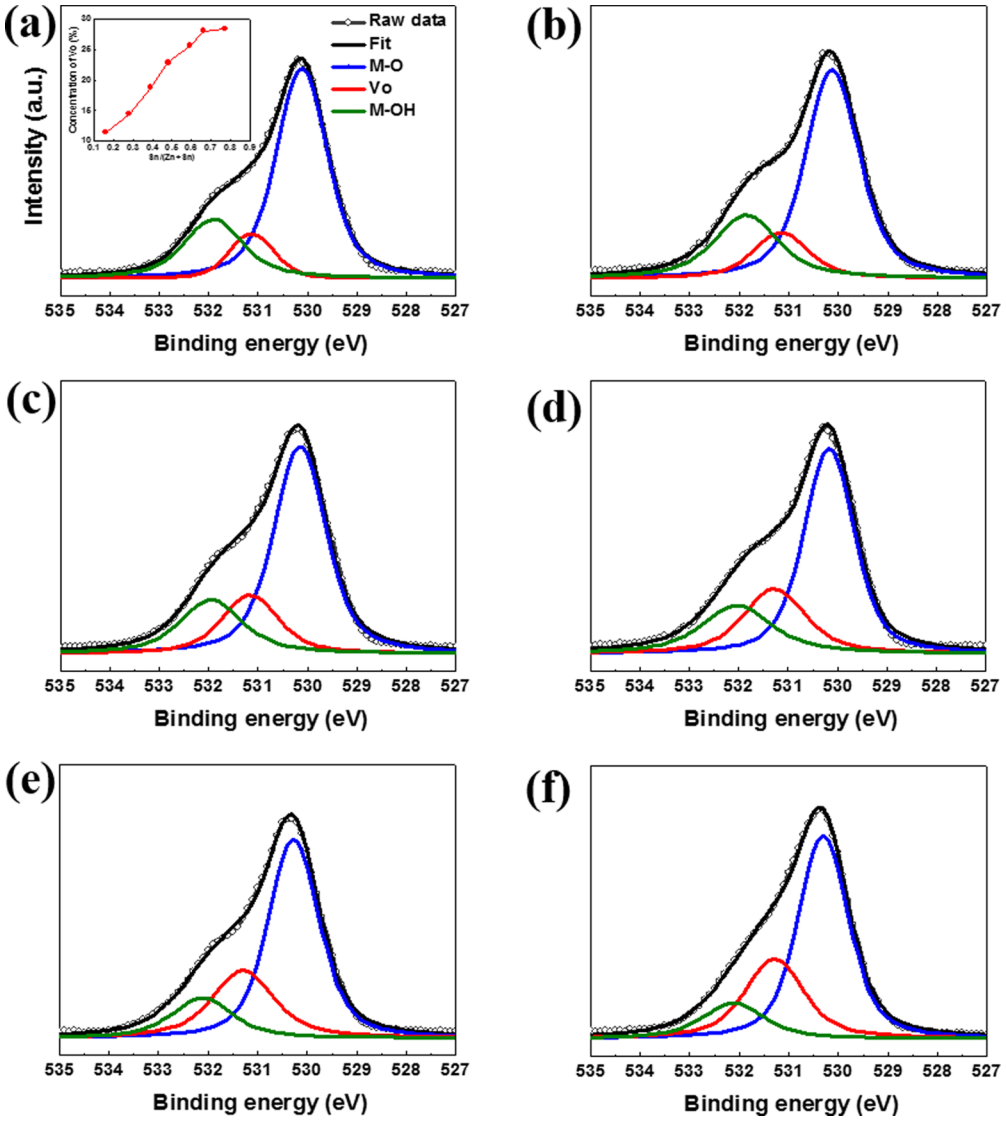

Figure 3. O 1s XP spectra and their deconvolution results of the ZTO films with a Sn/[Zn+Sn] ratio of (a) 0.16, (b) 0.28, (c) 0.39, (d) 0.48, (e) 0.59, and (f) 0.66. Inset in panel a shows the variation of V_O peak ratio as a function of Sn/[Zn+Sn].

The microstructural evolution of the ZTO thin films as a function of the Sn concentration was investigated further by HRTEM. Figure 2 shows the cross-sectional TEM images of the ZTO films with Sn/[Zn+Sn] ratios of 0.16, 0.48, and 0.77. The ZTO films with a Sn/[Zn+Sn] ratio of 0.48 were amorphous, which can be also confirmed by the amorphous halo ring in the selected area diffraction pattern. The amorphous nature of this ZTO film was observed in all scanned electron transparent region, indicating the complete amorphous phase of the ZTO film with a Sn/[Zn+Sn] ratio of 0.48. In contrast, the ZTO films with Sn/[Zn+Sn] ratios of 0.16 and 0.77 showed lattice fringes and the presence of grain boundaries, which is consistent with the GIXRD data.

The chemical states of the ZTO films with different Sn concentrations were examined by XPS. Figure 3 shows the O 1s XP spectra of the ZTO films with Sn/[Zn+Sn] ratios ranging from 0.16 to 0.66. The photoelectron binding energies were calibrated to the C 1s peak for the C−C bonds at 284.5 eV. The O 1s peak was deconvoluted into three peaks at 530.2, 531.2, and 531.9 eV.[23,24] The O 1s peaks centered at 530.2 eV was assigned to the oxygen bonded to fully coordinated metal ions (tetrahedrally coordinated in the case of Zn and octahedrally coordinated in the case of Sn) and the peak at 531.2 eV was assigned to the oxygen bonded to under-coordinated metal ions. In a crystal, the latter peak is associated with the oxygen vacancies (V_O). On the other hand, the oxygen vacancy cannot be strictly defined in the amorphous material, because of the lack of long-range order. However, for the sake of simplicity, the oxygen associated with under-coordinated metal ions will be referred as the V_O-related O 1s, even in amorphous phase ZTO film. The peak at 531.9 eV was assigned to impurity-related oxygen, such as hydroxyl groups. It is noted that the different assignment of O 1s XP spectra has been proposed, where the intermediate peak of O 1s XP spectra was assigned to the metal hydroxide.[6,25,26] In particular, Rajachidambaram et al. found that the intermediate peak of O 1s decreased substantially after the in situ high-temperature annealing at 550 °C in a vacuum chamber (P_{O_2} = 10^{-6} Torr).[25] During high-temperature vacuum annealing, the adsorbed species on the ZTO surface are likely to be desorbed. However, it is also expected that the ZTO film become denser, because of the viscous flow at high-temperature annealing,

Table 1. O 1*s* Peaks Deconvoluted from the XP Spectra of the Various ZTO Films with Different Sn/(Zn+Sn) Ratios. the Error Bar Denotes the Sample-to-Sample Variations of the Corresponding Peak Positions

	O 1s Peak [eV]		
Sn/(Zn+Sn)	lattice oxygen [O_O](530.2 ± 0.1 eV)	oxygen deficient [V_O](531.2 ± 0.1 eV)	Hydroxyl(531.9 ± 0.1 eV)
0.77	0.58	0.28	0.14
0.66	0.59	0.28	0.13
0.59	0.59	0.26	0.15
0.48	0.57	0.23	0.20
0.39	0.62	0.19	0.20
0.28	0.63	0.15	0.22
0.16	0.66	0.12	0.22

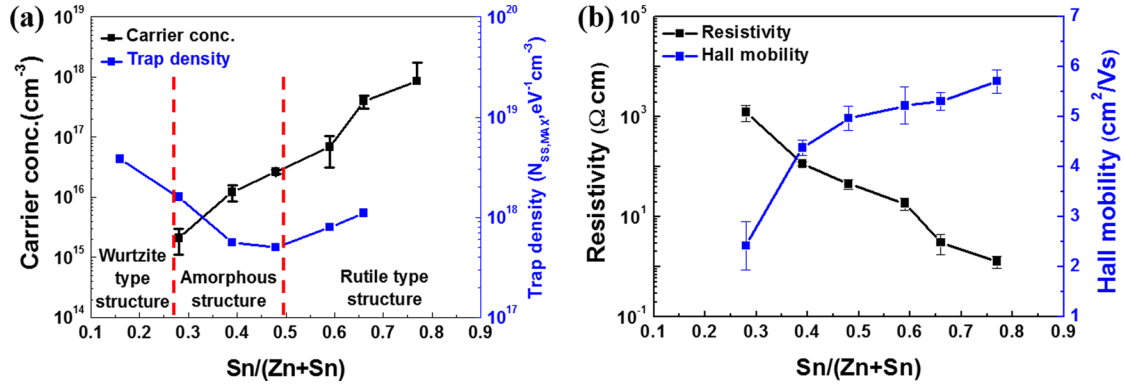

Figure 4. Variation of (a) the carrier concentration and trap density and (b) the resistivity and Hall mobility for the ZTO films, as a function of the Sn concentration.

which was not considered in their work. The densification would reduce the concentration of V_O in the ZTO film.[27,28] Therefore, exact assignment of the O 1s XP spectra needs further theoretical and experimental verification.

The relative areas of the oxygen vacancy (V_O)-related peak increased monotonically with increasing Sn/[Zn+Sn] ratio, as shown in Figure 3 and Table 1. The definition of V_O in amorphous material could be controversial. Therefore, V_O in this work corresponds to the broken bond with metal ions (or less-coordinated metal ions) and related local structural distortion. The area of the V_O-related peak area ratio for the ZTO film increased from 11.5% at a Sn/[Zn+Sn] ratio of 0.16 to 28.4% at a Sn/[Zn+Sn] ratio of 0.77. The inset in Figure 3a shows the variations in the relative area ratio of the V_O-related O 1s, as a function of the Sn concentration. Because the Sn−O bond is weaker than the Zn−O bond, V_O formation is enhanced with increasing Sn concentration in the ZTO film.[29,30] The role of V_O in the electrical properties of the MO TFTs is controversial. V_O can act as either a shallow donor center or a deep level trap, which depends on the species and coordination number (CN) of cations near the V_O.[31] At a fixed Sn concentration, the free electron density (n_e) of the ZTO film can be controlled experimentally by adjusting the oxygen ratio,[32−34] suggesting that some of the V_O are indeed shallow donors. Therefore, it is expected that the n_e value of the ZTO film increases with increasing Sn concentration.

While the O 1s XP spectra of ZTO films was strongly dependent on the Sn concentration, the binding energy and shape of Sn $3d_{5/2}$ XP spectra were relatively independent of the Sn concentration, as shown in Figure S1 in the Supporting Information (SI). The binding energy of the Sn $3d_{5/2}$ XP spectra peak was located at 486.5−486.6 eV, indicating that the Sn ions in the ZTO films are present as mostly Sn^{4+}. On the other hand, the concentration of OH and Cl impurities in the ZTO films decreased gradually with increasing Sn concentration, as shown in Table 1 and Figure S2 in the SI. In this study, the zinc acetate and tin chloride were used as the Zn and Sn atomic precursors, respectively. These results suggest that the hydrolysis and condensation reaction of metal complex, which is required to form the M-O-M lattice, are mainly limited by thermal decomposition of acetate in the Zn precursor rather than chlorine in the Sn precursor. Otherwise, the Cl concentration in the ZTO film would increase with increasing Sn concentration. Therefore, the increasing residual impurities such as metal hydroxide and Cl in the ZTO films with increasing Zn concentration can be attributed to the inefficient decomposition of organic acetate zinc precursor during the thermal annealing.

Figure 4 shows the change in n_e, resistivity, and Hall mobility estimated from the Hall measurements for the ZTO films as a function of the Sn concentration. The Hall data could not be measured for ZTO film with Sn/[Zn+Sn] = 0.16, because of the high electrical resistivity of ZTO film. The n_e increased with increasing Sn concentration, which is consistent with the aforementioned simple hypothesis. The Hall mobility of the ZTO films increased monotonically with increasing Sn concentration, which can be explained by the percolation conduction mechanism. Therefore, the resistivity of the ZTO films decreased substantially with increasing Sn concentration, as shown in Figure 4b. Interestingly, the n_e value of the ZTO film increased ~400 fold (from 2.1×10^{15} to 8.5×10^{17} cm^{-3}) with increasing the Sn/[Zn+Sn] ratio from 0.28 to 0.77, whereas the V_O concentration of the ZTO film estimated by XPS increased ~2-fold. This suggests that the ratio of a shallow V_O to a deep V_O depends on the Sn composition. The several tens % of V_O detected by XPS corresponds to a vacancy density

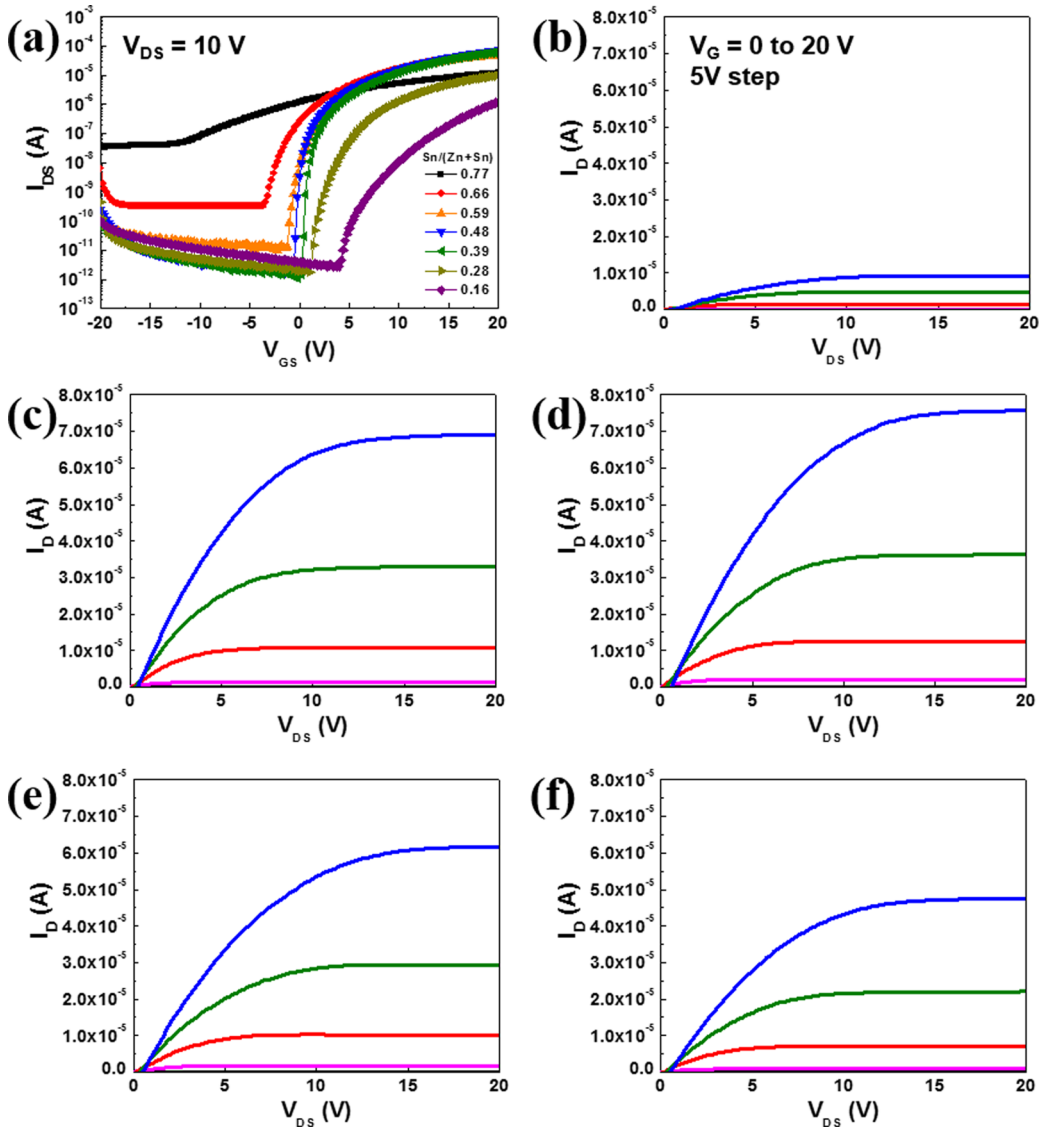

Figure 5. (a) Representative transfer characteristics of the ZTO TFTs for the different Sn concentrations. ALso shown are the output characteristics of the ZTO TFTs at Sn/[Zn+Sn] ratios of (b) 0.28, (c) 0.39, (d) 0.48, (e) 0.59, and (f) 0.66.

on the order of $10^{21}-10^{22}$ cm^{-3}. Such a high vacancy concentration does not represent the bulk of the film, because XPS mostly probes the chemical structure of a defective film surface. Nevertheless, the consistent trend in V_O with the Sn/[Zn+Sn] ratio suggests that the variation in n_e has a relationship with the V_O states. The different energy levels of V_O within the band gap of the ZTO film for different Sn/[Zn+Sn] ratios, rather than its concentration itself, are more responsible for the variation in n_e. The higher V_O concentration, in the film with a high Sn/[Zn+Sn] ratio introduces abundant shallow levels, resulting in a higher n_e. The energy levels of the V_O in the band gap of ZTO could vary according to the chemical environment near V_O. V_O with a higher CN of Sn has a shallow level, compared to V_O with a higher CN of Zn.[8,35] Therefore, with increasing Sn concentration, the energy level of V_O in the ZTO film becomes shallower (lower trap depth), resulting in an exponential increase in carrier generation with increasing Sn concentration, which corroborates the results shown in Figure 4a. On the other hand, this interpretation is valid only for the case where the host ZTO maintains an identical crystal (or amorphous) structure throughout the entire Sn concentration range. As observed by GIXRD and HRTEM, the ZTO films have a ZnO-like wurtzite structure, an amorphous structure, and SnO_2-like rutile structure, respectively, with increasing Sn concentration. This suggests that the aforementioned explanation for a higher n_e with increasing Sn concentration might be valid only for amorphous ZTO materials with the Sn/[Zn+Sn] ratios from 0.28 to 0.48, because the CN of an amorphous phase can vary almost linearly with the Sn concentration. In crystalline materials, the CN of V_O must be restricted by the structure of the specific crystal. Therefore, in crystalline materials, the following explanation must be more reasonable for the variation of n_e with Sn concentration.

The ZTO films with a high Sn/[Zn+Sn] ratios from 0.59 to 0.88 had a rutile SnO_2-like crystal structure, meaning that Zn atoms in this material are impurities. The Zn atom can substitute for the Sn site in the rutile ZTO film or be present as interstitial ions. The substitutional Zn (Zn''_{Sn}) can act as an acceptor center. On the other hand, Hall measurements showed that these films also have an *n*-type nature, suggesting that the majority carriers are electrons, which must be produced mainly by V_O formation. The highest Sn concentration in these

Table 2. Device Parameters Including μ_{FE}, SS, V_{th}, I_{on}/I_{off}, $D_{it,max}$, $N_{SS,max}$, and ΔV_{th} of the Various ZTO TFTs

Sn/(Zn+Sn)	μ_{FE} ($cm^2/(V\ s)$)	SS (V/decade)	V_{th} (V)	I_{on}/I_{off}	$D_{it,max}$ ($eV^{-1}cm^{-2}$)	$N_{SS,max}$ ($eV^{-1}cm^{-3}$)	ΔV_{th} (V)
0.16	0.5 ± 0.1	2.8 ± 0.24	8.5 ± 1.6	4.6×10^5	9.6×10^{12}	3.8×10^{18}	−3.6
0.28	0.9 ± 0.1	1.3 ± 0.08	3.1 ± 1.0	5.6×10^6	4.4×10^{12}	1.6×10^{18}	−2.4
0.39	4.0 ± 0.1	0.4 ± 0.03	0.8 ± 0.6	5.9×10^7	1.5×10^{12}	5.6×10^{17}	−3.0
0.48	4.3 ± 0.3	0.4 ± 0.02	0.0 ± 0.3	4.1×10^7	1.5×10^{12}	5.0×10^{17}	−3.9
0.59	3.3 ± 0.3	0.7 ± 0.02	−0.3 ± 0.1	5.1×10^6	2.4×10^{12}	8.0×10^{17}	−6.4
0.66	3.1 ± 0.2	1.1 ± 0.04	−2.7 ± 0.7	2.0×10^5	3.6×10^{12}	1.1×10^{18}	−10.3
0.77	0.3 ± 0.1			3.6×10^2			

ZTO films coincides with the highest tendency of V_O formation due to the weaker Sn−O bonds, compared to Zn−O bonds. Therefore, Zn''_{Sn} decreases the electron concentration by trapping them. Again, the larger decrease in carrier concentration (from 8.5×10^{17} cm^{-3} to 3.9×10^{17} cm^{-3}) when the Sn/[Zn+Sn] ratio is decreased from 0.77 to 0.66 (see Figure 4a) showed that the major contribution to the carrier concentration is the V_O concentration.

Figure 5a shows the representative transfer characteristic curves (I_{DS} vs V_{GS}) of the ZTO TFTs with different Sn concentrations when the drain voltage (V_{DS}) was set to 10 V. The field-effect carrier mobility (μ_{FE}) was determined from the slope of the $I_{DS}^{1/2}$ vs V_{GS} plot using the following equation:

$$I_{DS} = \left(\frac{WC_i}{2L}\right)\mu_{FE}(V_{GS} - V_{th})^2 \quad (2)$$

where L is the channel length, W the width, and C_i the gate capacitance per unit area. The threshold voltage (V_{th}) was defined as the gate voltage (V_{GS}) that induces a drain current of $L/W \times 10$ nA at V_{DS} = 10 V. The subthreshold swing (SS = $dV_{GS}/d\ \log I_{DS}$ [V/decade]) was extracted from the linear part of the $\log(I_{DS})$ vs V_{GS} plot. The fast bulk traps (N_{SS}) and semiconductor−insulator interfacial traps (D_{it}) were calculated using the following equation:[36]

$$SS = \frac{qk_BT(N_{SS}t_{ch} + D_{it})}{C_i \log(e)} \quad (3)$$

where q is the electron charge, k_B the Boltzmann constant, T the absolute temperature, and t_{ch} the channel layer thickness. N_{SS} and D_{it} in the ZTO TFTs were calculated by setting one of parameters to zero. Therefore, the N_{SS} and D_{it} values must be considered the maximum trap density formed in a given system. The carrier transport properties and current modulation capability of the devices were strongly dependent on the Sn concentration in the channel layer. The TFTs with Sn/[Zn+Sn] ratios of 0.16 and 0.28 commonly showed a low "on" current (I_{on}) in the highly positive V_{GS} region, whereas the "off" current (I_{off}) in the negative V_{GS} region was sufficiently low. This is related primarily to the very low carrier concentration (Figure 4) for these cases. The I_{on}/I_{off} ratio was only 4.5×10^5, μ_{FE} was 0.5 $cm^2/(V\ s)$, and V_{th} was as high as 8.5 V in the case of Sn/[Zn+Sn] = 0.16 (see Figure 5a and Table 2). With increasing Sn/[Zn+Sn] ratio of up to 0.48, the μ_{FE}, V_{th}, SS, and I_{on}/I_{off} ratio values of the device were improved substantially to 4.3 $cm^2/(V\ s)$, 0 V, 0.4 V/decade, and 4.1×10^7, respectively (see Table 2). Generally, the carrier transport in the conduction band of an amorphous ZTO film is dominated by the percolated path composed of Sn 5s orbitals, which must be improved by the higher Sn concentration in the ZTO film. On the other hand, in amorphous materials, the lower edge of the conduction band is not as clearly defined as that of the crystalline material. The lower edge region of the conduction band in amorphous semiconductor oxides is largely due to localized states, which form a mobility edge.[37] Under these circumstances, the higher carrier concentration is beneficial for achieving a higher apparent μ_{FE}. This is because the localized states with lower energy levels are filled with some of the carriers first, and the remaining carriers are transported via the states residing relatively far above the mobility edge.[9,38] Therefore, the enhancement of the device parameters in the Sn-deficient composition range is a reflection of the increasing n_e with increasing Sn doping level, which originates from either the creation of a shallow V_O center or the reduced N_{SS} value. When the Sn concentration was larger than a Sn/[Zn+Sn] ratio of 0.59, the μ_{FE} of the resulting device deteriorated again. For example, the device with a Sn/[Zn+Sn] ratio of 0.66 showed a low μ_{FE} of 3.1 $cm^2/(V\ s)$, even though its channel layer had a higher n_e of 3.9×10^{17} cm^{-3}. The Sn concentration-dependent mobility variation of the solution-processed ZTO devices was also observed clearly in the output characteristics (see Figures 5b−5f). The microstructure transition of the ZTO film from the amorphous phase to the polycrystalline state is likely to be responsible for this adverse effect. The two-dimensional (2D) defect states in the grain boundary of a polycrystalline rutile ZTO film can act as a tailing state below the conduction band minima, which cause the additional scattering of charge carriers, leading to a decrease in μ_{FE}. The TFT with a Sn/[Zn+Sn] ratio greater than ~0.66 generally showed high I_{off} in the negative V_{GS} region with highly negatively shifted V_{th} values. The TFT with the highest Sn/[Zn+Sn] ratio of 0.77 could not be turned off, even with a high negative V_{GS}. This can be attributed to the excessively high carrier concentration and high defect density in these channel materials.

It is interesting to note that the trap density of the ZTO TFTs exhibited the U-shape curve and the minimum value of 5.0×10^{17} was observed for the device at the Sn/[Zn+Sn] of 0.48 (see Figure 4a). As previously mentioned, the residual impurities originated from the metal precursors decreased gradually with increasing Sn concentration. Because these residual impurities are known to act as the trapping center of charge carriers, the decreasing N_{SS} values of the ZTO TFTs in the amorphous Sn-deficient composition range partly reflect the reduced impurities with increasing Sn doping level (see Figure 4a). In contrast, the increasing N_{SS} tendency in the polycrystalline Sn-rich ZTO TFTs can be attributed to the increasing V_O defect and the grain-boundary-related defects density, rather than the variation of residual impurities in the ZTO film.

Finally, the negative bias illumination stress (NBIS) instability of the solution-processed ZTO TFTs with different Sn concentrations was examined. The NBIS instability is an important performance measure because the application of MO TFTs in transparent electronics inevitably involves long

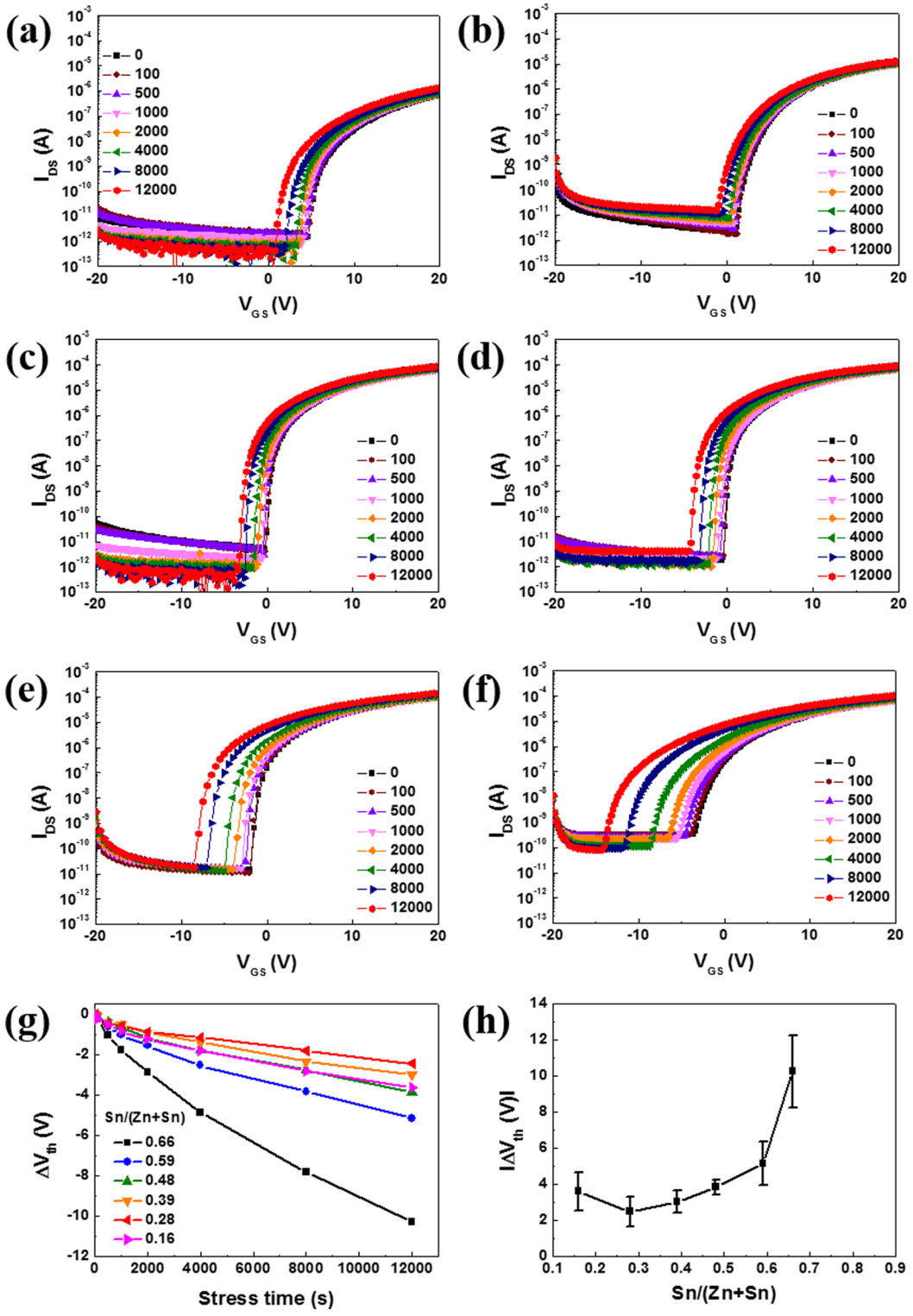

Figure 6. Evolution of the transfer characteristics of ZTO TFTs with a Sn/[Zn+Sn] ratio of (a) 0.16, (b) 0.28, (c) 0.39, (d) 0.48, (e) 0.59, and (f) 0.66, as a function of the NBIS time. Also shown are the variations in V_{th} as a function of (g) the NBIS time and (h) the incorporated Sn concentration.

exposure to light stress on the semiconducting oxide semiconductor films under the negative V_{GS} condition.[7] The devices exhibited significant instability under the NBIS condition. Figures 6a–f show the evolution of the transfer curves for the various ZTO TFTs (Sn/[Zn+Sn] ratio = 0.16–0.66) for the different NBIS times (up to 12 000 s) under the following conditions: V_{GS} and V_{DS} of −20 and 10 V, respectively, at room temperature with an illumination power intensity of ∼2.0 mW/cm^2 and a wavelength of ∼500 nm, which was filtered from a white-light halogen lamp. The NBIS-induced V_{th} variation was dependent on the Sn concentration in the ZTO film. Figure 6g summarizes the variations in V_{th} of the various TFTs as a function of the stress time, and Figure 6h shows the maximum V_{th} variation at a stress time of 12 000 s. The most desirable

dx.doi.org/10.1021/am503351e | ACS Appl. Mater. Interfaces 2014, 6, 14026–14036

NBIS stability was achieved from the TFT with a Sn/[Zn+Sn] ratio of 0.28 (the V_{th} shift was −2.4 V after a stress time of 12 000 s), whereas an increasing or decreasing Sn concentration degraded it. The degradation in the NBIS stability was considerably more severe when the Sn concentration was higher (V_{th} shift was −10.3 V after a stress time of 12 000 s).

The NBIS induced V_{th} instability of the MO TFTs was attributed to photocreated hole trapping,[39] the phototransition of V_O, and subsequent drift of ionized V_O,[40] or the photodesorption of oxygen molecules on the back surface.[34] The latter mechanism can be excluded because the ZTO channel layer in this study was encapsulated by the PMMA film. The first hole trapping model is unlikely to be responsible for this observation. The creation of electron and hole pairs via a band-to-band transition was not expected because the energy of photon used as a light source (2.48 eV) is lower than the band-gap energy (3.2−3.8 eV) of the ZTO films. Therefore, the Sn concentration-dependent NBIS instability of the ZTO TFTs seems to be strongly related to the V_O related mechanism. The deep V_O defect can be excited to the ionized V_O^{2+} by the light exposure, which donates two free electrons in the conduction band of oxide semiconductor materials. This causes a negative V_{th} shift in the resulting devices, even when the measurement was performed under the no illumination condition, because of the very long recombination time of such photoinduced carriers.[41] The photoconversion of V_O to V_O^{2+} will be proportional to the concentration of pre-existing V_O. The potential migration of V_O^{2+} toward the semiconductor/insulator interface due to the applied NBS in the gate electrode also results in a negative V_{th} shift. As mentioned previously, the concentration of V_O in the ZTO film increased monotonously with increasing Sn concentration. Therefore, the amplification of NBIS instability in the ZTO TFTs with increasing Sn concentration, except for the case of the ZTO TFT with Sn/[Zn+Sn] ratio of 0.16, is consistent with the variation in the V_O concentration. The unexpected NBIS degradation of the device with Sn/[Zn+Sn] = 0.16 (ΔV_{th} = −3.6 V), compared to that with Sn/[Sn+Zn] = 0.28 (ΔV_{th} = −2.4 V) cannot be reconciled with its lower V_O density. This suggests that another degradation path exists. This deviation is presumably due to the accelerated migration of V_O^{2+} via the grain boundaries. The (002) columnar polycrystalline structure of the ZTO film with Sn/[Zn+Sn] = 0.16 would provide an effective and easy path for the migration of V_O^{2+} defects, because the diffusion of point defects in the grain boundary of a polycrystalline material is generally much faster than that in an amorphous material.[42,43] Indeed, the grain boundary-assisted V_O^{2+} migration and the accelerated NBIS-induced V_{th} degradation was also reported previously in indium zinc oxide TFTs.[44,45]

In the Sn-rich ZTO film with a Sn/[Zn+Sn] ratio of 0.66, the migration of V_O^{2+} defects is also enhanced by the grain boundaries of the polycrystalline material, which resulted in a huge negative V_{th} shift of −10.3 V, in addition to the high V_O concentration. The best transistor performance, in terms of the mobility, N_{SS}, and I_{on}/I_{off} ratio, was obtained for the device with Sn/[Zn+Sn] = 0.48, whereas the device with Sn/[Zn+Sn] = 0.28 exhibited the most stable behavior, in terms of the NBIS stability. Therefore, the oxygen vacancy concentration and net carrier density in the ZTO thin film are the important key parameters for the compromise between the performance and photobias stability of the resulting TFTs. In addition, the ZTO channel layer with a discernible polycrystalline structure is undesirable for a photobias-stable device, even when it has a lower oxygen vacancy concentration.

4. CONCLUSION

The structural, chemical, and electrical properties of the solution-processed zinc tin oxide (ZTO) films were examined at different Sn concentrations. The ZTO films with Sn/[Sn+Zn] ratios ranging from 0.28 to 0.48 exhibited an amorphous phase, whereas the Sn-deficient and excess ZTO films were in a polycrystalline phase with wurtzite and rutile structures, respectively. The V_O concentration and n_e values of the ZTO film increased monotonously with increasing Sn concentration. The resulting carrier transport properties of the ZTO TFTs improved as the Sn/[Zn+Sn] ratio was increased to 0.48. The TFT with a Sn/[Zn+Sn] ratio of 0.48 exhibited a mobility, SS, V_{th}, and I_{on}/I_{off} of 4.3 $cm^2/(V\ s)$, 0.4 V/decade, 0 V, and 4.1×10^7, respectively. These values are generally inferior to the best performance reported for vacuum-processed TFTs with a ZTO channel layer and a similar Sn/[Sn+Zn] ratio, but are still quite useful, considering the inexpensive and simple process flow, which is critical for the economic production of large-area flat-panel displays. In addition, the trend of the variations in the device performance of solution-processed ZTO TFTs according to the Sn/[Zn+Sn] ratio is analogous to that of vacuum-processed devices, suggesting that the properties reported in this study are genuine to the material. The resistance under the NBIS condition was maximized for the device with Sn/[Zn+Sn] = 0.28, which was determined by both the lower V_O concentration and amorphous phase of the ZTO films. The Sn-deficient and excess ZTO device suffered from a high negative V_{th} shift under negative bias illumination stress (NBIS) conditions as well as inferior transport properties, which could be attributed to the large defect concentration, such as V_O or residual impurities and/or polycrystalline phase nature.

■ ASSOCIATED CONTENT

Ⓢ Supporting Information

This material is available free of charge via the Internet at http://pubs.acs.org.

■ AUTHOR INFORMATION

Corresponding Authors

*E-mail: jkjeong@inha.ac.kr (J. K. Jeong).
*E-mail: cheolsh@snu.ac.kr (C. S. Hwang).
*E-mail: thinfilm@snu.ac.kr (H. J. Kim).

Notes

The authors declare no competing financial interest.

■ ACKNOWLEDGMENTS

This study was supported by the Industrial Strategic Technology Development Program Funded by MKE/MEIT (Nos. 10041808 and 10041041), the National Research Foundation of Korea (NRF) grant funded the Korean government (MEST) (Grant No. 2012 R1A2A2A0 2005854), and Converging Research Center Program (No. 2013K000158) through the Ministry of Science, ICT, and Future Planning, Korean government.

■ REFERENCES

(1) Nomura, K.; Ohta, H.; Takagi, A.; Kamiya, T.; Hirano, M.; Hosono, H. Room-Temperature Fabrication of Transparent Flexible

Thin-Film Transistors Using Amorphous Oxide Semiconductors. *Nature* **2004**, *432*, 488−492.
(2) Yabuta, H.; Sano, M.; Abe, K.; Aiba, T.; Den, T.; Kumomi, H.; Nomura, K.; Kamiya, T.; Hosono, H. High-Mobility Thin-Film Transistor with Amorphous $InGaZnO_4$ Channel Fabricated by Room Temperature RF-Magnetron Sputtering. *Appl. Phys. Lett.* **2006**, *89*, 112123.
(3) Suresh, A.; Wellenius, P.; Dhawan, A.; Muth, J. Room Temperature Pulsed Laser Deposited Indium Gallium Zinc Oxide Channel based Transparent Thin Film Transistors. *Appl. Phys. Lett.* **2007**, *90*, 123512.
(4) Levy, D. H.; Nelson, S. F.; Freeman, D. Oxide Electronics by Spatial Atomic Layer Deposition. *J. Disp. Technol.* **2009**, *5*, 484−494.
(5) Banger, K.; Yamashita, Y.; Mori, K.; Peterson, R.; Leedham, T.; Rickard, J.; Sirringhaus, H. Low-Temperature, High-Performance Solution-Processed Metal Oxide Thin-Film Transistors Formed by a "Sol−Gel on Chip" Process. *Nat. Mater.* **2010**, *10*, 45−50.
(6) Kim, M. G.; Kanatzidis, M. G.; Facchetti, A.; Marks, T. J. Low-Temperature Fabrication of High-Performance Metal Oxide Thin-Film Electronics via Combustion Processing. *Nat. Mater.* **2011**, *10*, 382−388.
(7) Jeong, J. K. Photo-Bias Instability of Metal Oxide Thin Film Transistors for Advanced Active Matrix Displays. *J. Mater. Res.* **2013**, *28*, 2071−2084.
(8) Kamiya, T.; Nomura, K.; Hosono, H. Present Status of Amorphous In−Ga−Zn−O Thin-Film Transistors. *Sci. Technol. Adv. Mater.* **2010**, *11*, 044305.
(9) Kamiya, T.; Nomura, K.; Hosono, H. Origins of High Mobility and Low Operation Voltage of Amorphous Oxide TFTs: Electronic Structure, Electron Transport, Defects and Doping*. *J. Disp. Technol.* **2009**, *5*, 468−483.
(10) Kim, D.; Koo, C. Y.; Song, K.; Jeong, Y.; Moon, J. Compositional Influence on Sol-Gel-Derived Amorphous Oxide Semiconductor Thin Film Transistors. *Appl. Phys. Lett.* **2009**, *95*, 103501.
(11) Lee, J.; Cho, D. Y.; Jung, J.; Kim, U. K.; Rha, S. H.; Hwang, C. S.; Choi, J. H. Theoretical and Experimental Studies on the Electronic Structure of Crystalline and Amorphous $ZnSnO_3$ Thin Films. *Appl. Phys. Lett.* **2013**, *102*, 242111.
(12) Hoffman, R. L. Effects of Channel Stoichiometry and Processing Temperature on the Electrical Characteristics of Zinc Tin Oxide Thin-Film Transistors. *Solid-State Electron.* **2006**, *5*, 784−787.
(13) McDowell, M. G.; Sanderson, R. J.; Hill, I. G. Combinatorial Study of Zinc Tin Oxide Thin-Film Transistors. *Appl. Phys. Lett.* **2008**, *92*, 013502.
(14) Chang, Y. J.; Lee, D. H.; Herman, G. S.; Chang, C. H. High-Performance, Spin-Coated Zinc Tin Oxide Thin-Film Transistors. *Electrochem. Solid-State Lett.* **2007**, *10*, H135−H138.
(15) Chiang, H. Q.; Wager, J. F.; Hoffman, R. L.; Jeong, J.; Keszler, D. A. High Mobility Transparent Thin-Film Transistors with Amorphous Zinc Tin Oxide Channel Layer. *Appl. Phys. Lett.* **2005**, *86*, 013503.
(16) Görrn, P.; Hölzer, P.; Riedl, T.; Kowalsky, W.; Wang, J.; Weimann, T.; Hinze, P.; Kipp, S. Stability of Transparent Zinc Tin Oxide Transistors under Bias Stress. *Appl. Phys. Lett.* **2007**, *90*, 063502.
(17) Jeong, S.; Jeong, Y.; Moon, J. Solution-Processed Zinc Tin Oxide Semiconductor for Thin-Film Transistors. *J. Phys. Chem. C* **2008**, *112*, 11082−11085.
(18) Kim, Y.-H.; Han, J.-I.; Park, S. K. Effect of Zinc/Tin Composition Ratio on the Operational Stability of Solution-Processed Zinc−Tin−Oxide Thin-Film Transistors. *IEEE Electron Device Lett.* **2012**, *33*, 50−52.
(19) Park, S. K.; Kim, Y.-H.; Kim, H.-S.; Han, J.-I. High Performance Solution-Processed and Lithographically Patterned Zinc−Tin Oxide Thin-Film Transistors with Good Operational Stability. *Electrochem. Solid-State Lett.* **2009**, *12*, H256−H258.
(20) Ryu, M. K.; Yang, S.; Park, S. H. K.; Hwang, C. S.; Jeong, J. K. Impact of Sn/Zn Ratio on the Gate Bias and Temperature-Induced Instability of Zn-In-Sn-O Thin Film Transistors. *Appl. Phys. Lett.* **2009**, *95*, 173508.
(21) Özgür, Ü.; Alivov, Y. I.; Liu, C.; Teke, A.; Reshchikov, M. A.; Doğan, S.; Avrutin, V.; Cho, S.-J.; Morkoç, H. A Comprehensive Review of ZnO Materials and Devices. *J. Appl. Phys.* **2005**, *98*, 041301.
(22) Jenkins, R.; Snyder, R. L. *Introduction to X-ray Powder Diffractometry*; Wiley: New York, 1996.
(23) Kim, M. G.; Kim, H. S.; Ha, Y. G.; He, J.; Kanatzidis, M. G.; Facchetti, A.; Marks, T. J. High-Performance Solution-Processed Amorphous Zinc−Indium−Tin Oxide Thin-Film Transistors. *J. Am. Chem. Soc.* **2010**, *132*, 10352−10364.
(24) Kim, Y. H.; Heo, J. S.; Kim, T. H.; Park, S.; Yoon, M. H.; Kim, J.; Oh, M. S.; Yi, G. R.; Noh, Y. Y.; Park, S. K. Flexible Metal-Oxide Devices Made by Room-Temperature Photochemical Activation of Sol−Gel Films. *Nature* **2012**, *489*, 128−32.
(25) Rajachidambaram, M. S.; Pandey, A.; Vilayurganapathy, S.; Nachimuthu, P.; Thevuthasan, S.; Herman, G. S. Improved Stability of Amorphous Zinc Tin Oxide Thin Film Transistors Using Molecular Passivation. *Appl. Phys. Lett.* **2013**, *103*, 171602.
(26) Nomura, K.; Kamiya, T.; Ikenaga, E.; Yanagi, H.; Kobayashi, K.; Hosono, H. Depth Analysis of Subgap Electronic States in Amorphous Oxide and Semiconductor, a-In−Ga−Zn−O, Studied by Hard X-Ray Photoelectron and Spectroscopy. *J. Appl. Phys.* **2011**, *109*, 073726.
(27) Kim, Y. J.; Yang, B. S.; Oh, S.; Han, S. J.; Lee, H. W.; Heo, J.; Jeong, J. K.; Kim, H. J. Photobias Instability of High Performance Solution Processed Amorphous Zinc Tin Oxide Transistors. *ACS Appl. Mater. Interfaces* **2013**, *5*, 3255.
(28) Rim, Y. S.; Jeong, W. H.; Kim, D. L.; Lim, H. S.; Kim, K. M.; Kim, H. J. Simultaneous Modification of Pyrolysis and Densification for Low-Temperature Solution-Processed Flexible Oxide Thin-Film Transistors. *J. Mater. Chem.* **2012**, *22*, 12491−12497.
(29) Kılıç, Ç.; Zunger, A. Origins of Coexistence of Conductivity and Transparency in SnO_2. *Phys. Rev. Lett.* **2002**, *88*, 095501.
(30) Noh, J.-Y.; Kim, H.; Nahm, H.-H.; Kim, Y.-S.; Kim, D. H.; Ahn, B.-D.; Lim, J.-H.; Kim, G. H.; Lee, J.-H.; Song, J. Cation Composition Effects on Electronic Structures of In-Sn-Zn-O Amorphous Semiconductors. *J. Appl. Phys.* **2013**, *113*, 183706.
(31) Kamiya, T.; Nomura, K.; Hirano, M.; Hosono, H. Electronic Structure of Oxygen Deficient Amorphous Oxide Semiconductor a-$InGaZnO_{4-X}$: Optical Analyses and First-Principle Calculations. *Phys. Status Solidi C* **2008**, *5*, 3098−3100.
(32) Ji, K. H.; Kim, J. I.; Jung, H. Y.; Park, S. Y.; Choi, R.; Kim, U. K.; Hwang, C. S.; Lee, D.; Hwang, H.; Jeong, J. K. Effect of High-Pressure Oxygen Annealing on Negative Bias Illumination Stress-Induced Instability of InGaZnO Thin Film Transistors. *Appl. Phys. Lett.* **2011**, *98*, 103509.
(33) Yang, B. S.; Park, S.; Oh, S.; Kim, Y. J.; Jeong, J. K.; Hwang, C. S.; Kim, H. J. Improvement of the Photo-Bias Stability of the Zn−Sn−O Field Effect Transistors by an Ozone Treatment. *J. Mater. Chem.* **2012**, *22*, 10994−10998.
(34) Yang, S.; Ji, K. H.; Kim, U. K.; Hwang, C. S.; Park, S. H. K.; Hwang, C. S.; Jang, J.; Jeong, J. K. Suppression in the Negative Bias Illumination Instability of Zn-Sn-O Transistor Using Oxygen Plasma Treatment. *Appl. Phys. Lett.* **2011**, *99*, 102103.
(35) Ágoston, P.; Albe, K.; Nieminen, R. M.; Puska, M. J. Intrinsic N-Type Behavior in Transparent Conducting Oxides: A Comparative Hybrid-Functional Study of In_2O_3, SnO_2, and ZnO. *Phys. Rev. Lett.* **2009**, *103*, 245501.
(36) Greve, D. W. *Field Effect Devices and Applications: Devices for Portable, Low-Power, and Imaging Systems*; Prentice Hall: Upper Saddle River, NJ, 1998; p xiv (379 pp).
(37) Anderson, P. Model for the Electronic Structure of Amorphous Semiconductors. *Phys. Rev. Lett.* **1975**, *34*, 953.
(38) Hosono, H. Ionic Amorphous Oxide Semiconductors: Material Design, Carrier Transport, and Device Application. *J. Non-Cryst. Solids* **2006**, *352*, 851−858.
(39) Ji, K. H.; Kim, J. I.; Mo, Y. G.; Jeong, J. H.; Yang, S.; Hwang, C. S.; Park, S. H. K.; Ryu, M. K.; Lee, S. Y.; Jeong, J. K. Comparative Study on Light-Induced Bias Stress Instability of IGZO Transistors

with SiNx and SiO_2 Gate Dielectrics. *IEEE Electron Device Lett.* **2010**, *31*, 1404−1406.
(40) Chowdhury, M. D. H.; Migliorato, P.; Jang, J. Light Induced Instabilities in Amorphous Indium−Gallium−Zinc−Oxide Thin-Film Transistors. *Appl. Phys. Lett.* **2010**, *97*, 173506.
(41) Ghaffarzadeh, K.; Nathan, A.; Robertson, J.; Kim, S.; Jeon, S.; Kim, C.; Chung, U.-I.; Lee, J.-H. Persistent Photoconductivity in Hf−In−Zn−O Thin Film Transistors. *Appl. Phys. Lett.* **2010**, *97*, 143510.
(42) Cao, M.; Voorde, P. V.; Cox, M.; Greene, W. Boron Diffusion and Penetration in Ultrathin Oxide with Poly-Si Gate. *IEEE Electron Device Lett.* **1998**, *19*, 291−293.
(43) Doyle, B. L.; Peercy, P. S.; Wiley, J. D.; Perepezko, J. H.; Nordman, J. E. Au Diffusion in Amorphous and Polycrystalline $Ni_{0.55}Nb_{0.45}$. *J. Appl. Phys.* **1982**, *53*, 6186−6190.
(44) Oh, S.; Yang, B. S.; Kim, Y. J.; Choi, Y. J.; Kim, U. K.; Han, S. J.; Lee, H. W.; Kim, H. J.; Kim, S.; Jeong, J. K. Dynamics of Negative Bias Thermal Stress-Induced Threshold Voltage Shifts in Indium Zinc Oxide Transistors: Impact of the Crystalline Structure on the Activation Energy Barrier. *J. Phys. D: Appl. Phys.* **2014**, *47*, 165103.
(45) Oh, S.; Yang, B. S.; Kim, Y. J.; Oh, M. S.; Jang, M.; Yang, H.; Jeong, J. K.; Hwang, C. S.; Kim, H. J. Anomalous Behavior of Negative Bias Illumination Stress Instability in an Indium Zinc Oxide Transistor: A Cation Combinatorial Approach. *Appl. Phys. Lett.* **2012**, *101*, 092107.